

Electron-Phonon Interactions in Bilayer Graphene: A First Principles Approach

K. M. Borysenko,¹ J. T. Mullen,² X. Li,¹ Y. G. Semenov,¹ J. M. Zavada,¹ M. Buongiorno Nardelli,^{2,3} and K. W. Kim^{1,*}

¹*Department of Electrical and Computer Engineering,
North Carolina State University, Raleigh, NC 27695-7911*

²*Department of Physics, North Carolina State University, Raleigh, NC 27695-8202*

³*CSMD, Oak Ridge National Laboratory, Oak Ridge, TN 37831*

Abstract

Density functional perturbation theory is used to analyze electron-phonon interaction in bilayer graphene. The results show that phonon scattering in bilayer graphene bears more resemblance with bulk graphite than monolayer graphene. In particular, electron-phonon scattering in the lowest conduction band is dominated by six lowest (acoustic and acoustic-like) phonon branches with only minor contributions from optical modes. The total scattering rate at low/moderate electron energies can be described by a simple two-phonon model in the deformation potential approximation with effective constants $D_{ac} \approx 15$ eV and $D_{op} \approx 2.8 \times 10^8$ eV/cm for acoustic and optical phonons, respectively. With much enhanced acoustic phonon scattering, the low field mobility of bilayer graphene is expected to be significantly smaller than that of monolayer graphene.

PACS numbers: 72.80.Vp, 71.38.-k, 71.15.Mb, 63.22.Rc

Graphene, a two-dimensional sheet of carbon atoms in a honeycomb lattice, has received wide attention due to its unique properties [1]. In addition to the significant interest in fundamental physics, which stems in part from the relativistic-like behavior of charge carriers, this material is considered very promising in many applications. Particularly, the possibility of manipulating the band gap in a bilayer form [2] offers an additional control for nonlinear functionality.

While there has been a large number of reports (both experimental and theoretical) on graphene and its derivatives [3–6], most of the studies on electron transport properties have concentrated on monolayer graphene (MLG). Among those requiring further investigation in bilayer graphene (BLG), intrinsic carrier-phonon scattering is one of the most crucial as it determines the ultimate limit of any electronic applications. Due to the nonpolar nature of the material, the deformation potential approximation is commonly used. However, the deformation potential constant that quantifies the strength of electron-phonon coupling, must be determined outside the developed theory, in the form of an empirical fitting parameter. The experimental results lie in a broad range (e.g., $D = 10 - 50$ eV) [4, 6] and further improvement of accuracy is essential for reliable analysis of transport characteristics. The *ab initio* numerical methods provide an alternative approach in addressing this problem as demonstrated successfully in MLG [7, 8]. In this study, we conduct a first principles calculation of electron-phonon interaction in BLG with AB (also known as Bernal) stacking. Specifically, the density functional perturbation theory (DFPT) is used to obtain the crystal phonon spectra and electron-phonon coupling matrix elements. The results illustrate the differences with MLG, indicating significant discrepancies in transport properties.

Although it has been reported that the electron-phonon matrix elements in MLG can be estimated with an excellent accuracy using the GW approximation [7] for the phonon modes associated with the observed Kohn anomalies [9], a considerably longer (compared to the DFPT) calculation time that the GW method requires, as well as the fact that the accuracy of DFPT is sufficient in many applications including carrier transport, justifies the use of DFPT for calculating electron-phonon matrix elements in BLG. We also demonstrate that the Kohn anomalies that lead to the largest discrepancy between DFPT and GW results, do not play an important role in the intrinsic electron scattering in BLG and so the accuracy of the calculated matrix elements is not essential in this case.

Figure 1 shows the calculated phonon dispersion $\omega_{\mathbf{q}}'$ along the Γ - K direction. Since

there are four carbon atoms in the unit cell, BLG has 12 phonon branches. However, only six lines are distinguishable across the entire first Brillouin zone (FBZ) as each of them are doubly degenerate due to the weak van der Waals coupling between the two carbon layers. The only exception, when the splitting has an appreciable magnitude, is the case of ZA (acoustic out-of-plane) and ZO' ("layer breathing") modes near the FBZ center. In addition, two other modes deviate from the pure acoustic nature with very small non-zero frequencies at the Γ point as shown in Fig. 1(b) (denoted as TA2 and LA2). Hence, only three branches are truly acoustic (ZA, TA1, LA1), while we will use a term "antisymmetric acoustic" to refer to the three low-frequency counterparts with acoustic-like behavior (ZO', TA2, LA2). Their polarization eigenvectors are akin to those of the acoustic modes in MLG, with the atomic displacements in two layers having opposite phase (hence "antisymmetric"). A similar terminology has been used in Raman spectroscopy studies [10].

The electron spectrum $E_{\mathbf{k}}^i$ of BLG has two close conduction bands (π_1^* and π_2^*); the distance between the bottoms of π_1^* and π_2^* is found to be in a range 0.35 – 0.4 eV [10–12]. The accurate estimate of the intrinsic electron scattering in BLG requires taking into account all four possible scattering scenarios: intraband ($\pi_1^* \rightarrow \pi_1^*$, $\pi_2^* \rightarrow \pi_2^*$), and interband ($\pi_1^* \rightleftharpoons \pi_2^*$). Correspondingly, we calculate four sets of matrix elements $|g_{\mathbf{k}+\mathbf{q},\mathbf{k}}^{(i,j)\nu}|$ that represent the quantum mechanical probability of electron transition from the state (i, \mathbf{k}) to $(j, \mathbf{k} + \mathbf{q})$, where i and j are the initial and final energy band respectively. The matrix element is calculated only for wave vectors \mathbf{q} in the irreducible Brillouin zone. However it is easy to obtain the matrix elements in the entire FBZ, by restoring the star of each \mathbf{q} -vector from the irreducible zone (which requires applying corresponding symmetry operations to the vectors \mathbf{q} and \mathbf{k} simultaneously). The result of this calculation for intraband scattering (when the electron is at the bottom of π_1^* , i.e. $\mathbf{k} = K$) is shown in Fig. 2. It is not surprising that MLG-like phonon modes (ZA, TA1, LA1, ZO1, TO1, LO1) and their BLG-counterparts (ZO', TA2, LA2, ZO2, TO2, LO2) have very similar electron-phonon matrix elements throughout FBZ. The difference is only exhibited in some cases, in points of high symmetry ($\mathbf{q} = \mathbf{K}$ and $\mathbf{q} = 0$). This can be explained by selection rules that apply to phonon-mediated electron transitions, and it results from different symmetries of atomic displacements of these two sets of modes [13]. As compared to MLG, the matrix elements have the same order of magnitude. The essential difference between matrix elements of MLG and the ones shown in Fig. 2 is that none of the in-plane optical phonon modes of BLG reveal Kohn anomalies

that were reported to be observed in a form of singularities at points $\mathbf{q} = \mathbf{K}$ and $\mathbf{q} = 0$ [8]. However, further calculations have shown that strong peaks similar to those found in MLG occur in the corresponding matrix elements of *interband* scattering $\pi_1^* \rightarrow \pi_2^*$. Figure 3 shows the matrix element of interband scattering $\pi_1^* \rightarrow \pi_2^*$ due to the phonons of branches 9 and 10 (TO1 and TO2). The symmetry analysis of these two branches imposes a selection rule that allows only participation of one of the two phonons with $\mathbf{q} = \mathbf{K}$ [13]. In agreement with this prediction, the sharp peaks at $\mathbf{q} = \mathbf{K}$ are observed only in the case of TO1. At the same time, the other Kohn anomaly (at $\mathbf{q} = 0$) is present in matrix elements of all four MLG-like optical branches: TO1, TO2, LO1, LO2 (see Fig. 3).

Based on the obtained matrix elements, the electron scattering rates are calculated using Fermi's golden rule

$$\left(\frac{1}{\tau}\right)_{\mathbf{k}}^{(i,j)\nu} = \frac{2\pi}{\hbar} \sum_{\mathbf{q}} \left| g_{\mathbf{k}+\mathbf{q},\mathbf{k}}^{(i,j)\nu} \right|^2 \Delta_{\mathbf{k},\mathbf{q}}^{(i,j)\nu}, \quad (1)$$

where $\Delta_{\mathbf{k},\mathbf{q}}^{(i,j)\nu} = (N_{\mathbf{q}}^{\nu} + \frac{1}{2} \pm \frac{1}{2}) \delta(E_{\mathbf{k}+\mathbf{q}}^j - E_{\mathbf{k}}^i \pm \hbar\omega_{\mathbf{q}}^{\nu})$, $N_{\mathbf{q}}^{\nu}$ is the phonon population factor, and the sign plus (minus) corresponds to the emission (absorption) of the phonon $\omega_{\mathbf{q}}^{\nu}$. The temperature dependence of the scattering rate stems only from the the numbers of phonons as we sum over wave vectors \mathbf{q} in the FBZ. Preliminary estimates confirm that the scattering rate, as a function of the initial electron state \mathbf{k} in the vicinity of the Dirac point \mathbf{K} , exhibits isotropy. Therefore we only consider the $K - \Gamma$ direction in \mathbf{k} -space and can represent τ^{-1} as a function of electron energy.

In the integration over FBZ the tight binding approximation was used to describe the electron energy spectrum $E_{\mathbf{k}}$ in BLG [1]. The second conduction band (π_2^*) has nearly the same shape as the lowest conduction band (π_1^*) near Dirac point \mathbf{K} : it is parabolic in close vicinity of $\mathbf{k} = \mathbf{K}$ and quasi-linear beyond that. The quasi-linear approximation holds true for quite high electron energies and therefore, this description appears sufficient in most calculations. In the tight binding approximation, the distance between the bottoms of π_1^* and π_2^* is γ_1 , which is the interlayer hopping integral in BLG (we use standard notations known as the Slonczewski-Weiss-McClure parametrization model [14, 15]). A recent resonant Raman studies show the result $\gamma_1 \simeq 0.4$ eV [11, 12], which is the value used in our calculation.

Figure 4 shows the total scattering rates associated with all four possible scenarios involving two conduction bands. Since the recent Raman experiments in BLG have shown the Kohn anomalies located in the q-points of high symmetry, one might expect their sig-

nificance in the overall picture of electron-phonon scattering in BLG. The separate analysis of different phonon branches in BLG, however, shows a qualitatively different picture. In case of intraband scattering in the lowest conduction band (π_1^*) the scattering rate due to absorption or emission of MLG-like optical phonons (ZO1, ZO2, TO1, TO2, LO1, LO2) is negligibly small in a wide range of energies ($E < 0.7$ eV). An explanation for this result comes directly from comparison of corresponding matrix elements of MLG [8] and those of BLG for $\pi_1^* \rightarrow \pi_1^*$ scattering: in the latter case the sharp peaks are missing. The Kohn anomalies similar to those in matrix elements of MLG, were observed in BLG - in the interband scattering $\pi_1^* \rightarrow \pi_2^*$ (see Fig. 3). However, the corresponding scattering rates have proven to be negligibly low. This result can be understood if one compares electron dispersions in MLG (π^*) and BLG (π_1^* and π_2^*). A simple analysis demonstrates that electron transitions $\pi_1^* \rightarrow \pi_2^*$ involving phonons $\mathbf{q} = 0$ and $\mathbf{q} = \mathbf{K}$ (where the anomalies occur) are prohibited by the energy and momentum conservation laws. In other words, the contour of integration from Eq. (1) never crosses (or comes close to) the peaks at the points Γ and K observed in the matrix element of BLG. The estimated minimal distance between this curve (which can be approximated by a circle) and the point $\mathbf{q} = \mathbf{K}$, is $0.034 (2\pi/a)$ for emission and $0.014 (2\pi/a)$ for absorption. For comparison, the analogous distance in case of intervalley scattering due to TO phonons in MLG, is much smaller, $\sim 10^{-7} (2\pi/a)$, which ensures the dominant role of the corresponding modes in electron scattering. The same consideration shows that the TO1 phonon with $\mathbf{q} = 0$ cannot influence the interband scattering in BLG. As a result, the total scattering rate in BLG, when the electron is initially in π_1^* (i.e., $\pi_1^* \rightarrow \{\pi_1^*, \pi_2^*\}$) is somewhat smaller at higher energies ($E_k \gtrsim 200$ meV), if compared to the total rate in MLG (see Fig. 4).

On the other hand, the low-energy scattering rate in BLG is substantially higher, which can be explained by a larger density of states in the vicinity of the Dirac point. More specifically, the density of state tends to zero linearly for the massless Dirac fermions of MLG while it is a constant in BLG as $\mathbf{k} \rightarrow K$. This non-zero density of states at the bottom of π_1^* and π_2^* leads to a peculiar effect. In MLG, the intravalley scattering on acoustic phonons can be treated as quasielastic as it was shown previously [16, 17]; only the modes with $\mathbf{q} \rightarrow 0$ can participate. As a result, the scattering rate is a linear function of energy that vanishes as $E_k \rightarrow 0$. In BLG, however, the intravalley scattering with absorption of acoustic phonon shows a different behavior. Aside from $\mathbf{q} = 0$, the energy and

momentum conservation in the electron scattering allows an additional solution - a circle with radius $|\mathbf{q}| = q_c = v_s \gamma_1 / \hbar v_F^2$. In the case of antisymmetric acoustic modes, an equivalent solution exists - a circle of radius $q_c = \sqrt{\gamma_1 \omega_\Gamma / \hbar v_F^2}$, where ω_Γ is the non-zero frequency of an antisymmetric acoustic mode in Γ -point. This leads to a non-zero absorption rate even at zero electron energies. It is important to emphasize that even though the deformation potential approximation can be used to describe electron-phonon coupling in BLG [6], the intravalley scattering cannot be treated as quasi-elastic due to the additional solution with $\mathbf{q} \neq 0$. The estimated value of the deformation potential constant in BLG is $D \approx 15$ eV, if we chose the TA2 branch as dominant [18]. This is much closer to the value obtained for graphite ($D \approx 16$ eV [19]) than that for MLG ($D \approx 4.5 - 5$ eV [8]). The scattering rates in BLG and graphite [20] turn out to be quite similar as well. The same dominant intrinsic scattering mechanism in graphite and BLG is intravalley transitions due to absorption and emission of acoustic phonons, while the contribution of the optical phonons is of secondary importance. In particular, $D_{op} \approx 2.8 \times 10^8$ eV/cm for the optical phonons in BLG, which is almost one order of magnitude smaller than in MLG [8, 18]. With much enhanced acoustic phonon scattering at low energies, the low field mobility of bilayer graphene is expected to be significantly smaller than that of monolayer graphene.

In summary, we have studied the electron-phonon interaction in BLG with AB stacking and found that the scattering rates exhibit qualitatively different behavior, if compared to MLG. As a result of a different electron spectrum (and thus, the density of states) in conduction bands of BLG, the intraband (π_1^*) scattering rates due to absorption of acoustic and antisymmetric acoustic phonons at low electron energies have quite large values ($\sim 10^9 - 10^{10}$ s $^{-1}$). The calculations confirmed that this scattering mechanism remains dominant in BLG, at all relevant electron energies in π_1^* — the property that is not observed in MLG. In π_2^* , the scattering rate is approximately a constant, $\approx 5 \times 10^{12}$ s $^{-1}$. The overall picture of electron-phonon coupling in BLG has more in common with that of the bulk graphite than it does with MLG. The estimated values of the deformation potential constants are $D \approx 15$ eV and $D_{op} \approx 2.8 \times 10^8$ eV/cm, for acoustic and optical phonons respectively.

This work was supported, in part, by the DARPA/HRL CERA, ARL, and SRC/FCRP FENA programs. MBN wishes to acknowledge partial support from the Office of Basic Energy Sciences, US DOE at Oak Ridge National Lab under contract DE-AC05-00OR22725 with UT-Battelle, LLC. JMZ acknowledges support from NSF under the IR/D program.

* Electronic address: kwk@ncsu.edu

- [1] A. H. Castro Neto, F. Guinea, N. M. R. Peres, K. S. Novoselov, and A. K. Geim, *Rev. Mod. Phys.* **81**, No. 1 (2009).
- [2] E. V Castro, K. S. Novoselov, S. V. Morozov, N. M. R. Peres, J. M. B. Lopes dos Santos, J. Nilsson, F. Guinea, A. K. Geim, and A. H. Castro Neto, *J. Phys.: Condens. Matter* **22**, 175503 (2010).
- [3] J.-H. Chen, C. Jang, M. Ishigami, S. Xiao, E. D. Williams, and M. S. Fuhrer, *Solid State Commun.* **149**, 1080 (2009).
- [4] E. H. Hwang and S. Das Sarma, *Phys. Rev. B* **75**, 205418 (2007).
- [5] E. H. Hwang and S. Das Sarma, *Phys. Rev. Lett.* **101**, 156802 (2008).
- [6] J. K. Viljas and T. T. Heikkilä, *Phys. Rev. B* **81**, 245404 (2010).
- [7] M. Lazzeri, C. Attaccalite, L. Wirtz, and F. Mauri, *Phys. Rev. B* **78**, 081406 (2008).
- [8] K. M. Borysenko, J. T. Mullen, E. A. Barry, S. Paul, Y. G. Semenov, J. M. Zavada, M. Buongiorno Nardelli, and K. W. Kim, *Phys. Rev. B* **81**, 121412(R) (2010).
- [9] W. Kohn, *Phys. Rev. Lett.* **2**, 393 (1959).
- [10] D. L. Mafra, L. M. Malard, S. K. Doorn, H. Htoon, J. Nilsson, A. H. Castro Neto, and M. A. Pimenta, *Phys. Rev. B* **80**, 241414 (2009).
- [11] A. Das, B. Chakraborty, S. Piscanec, S. Pisana, A. K. Sood, and A. C. Ferrari, *Phys. Rev. B* **79**, 155417 (2009).
- [12] Z. Q. Li, E. A. Henriksen, Z. Jiang, Z. Hao, M. C. Martin, P. Kim, H. L. Stormer, and D. N. Basov, *Phys. Rev. Lett.* **102**, 037403 (2009).
- [13] L. M. Malard, M. H. D. Guimarães, D. L. Mafra, M. S. C. Mazzoni, and A. Jorio, *Phys. Rev. B* **79**, 125426 (2009).
- [14] J. W. McClure, *Phys. Rev.* **108**, 612 (1957).
- [15] J. C. Slonczewski and P. R. Weiss, *Phys. Rev.* **109**, 272 (1958).
- [16] F. T. Vasko and V. Ryzhii, *Phys. Rev. B* **76**, 233404 (2007).
- [17] E. H. Hwang and S. Das Sarma, *Phys. Rev. B* **77**, 115449 (2008).
- [18] The best fitting results for the total scattering rate are achieved when the antisymmetric acoustic branch TA2, and optical branch TO2 are chosen, with the effective deformation potential

constants $D \approx 15$ eV and $D_{op} \approx 2.8 \times 10^8$ eV/cm, respectively. There are six acoustic-like (ZA, ZO', TA1, TA2, LA1, LA2) and four optical (TO1, TO2, LO1, LO2) vibrational modes in BLG that contribute almost equally in a wide range of energies. Thus, the branches TA2 and TO2 were chosen simply to ensure the best fit, and not because of their exceptional role.

- [19] K. Sugihara, Phys. Rev. B **28**, 2157 (1983).
- [20] J. Jiang, R. Saito, A. Grüneis, G. Dresselhaus, and M. S. Dresselhaus, Chem. Phys. Lett. **392**, 383 (2004).

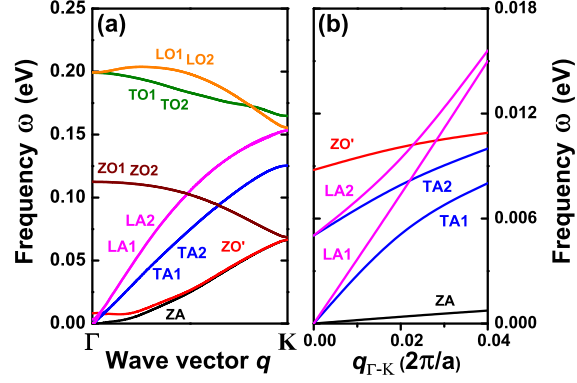


FIG. 1: (Color online) The phonon spectrum of BLG along the line $\Gamma - K$, obtained by DFPT method (a). There are total of 12 phonon branches in BLG - twice as many as in MLG. But the weak van der Waals interlayer coupling results in effective double degeneracy of every branch, everywhere in FBZ except the vicinity of Γ -point where a small splitting is exhibited in case of first six branches (b). The largest splitting occurs between two out-of-plane branches: ZA and ZO' ("breathing mode").

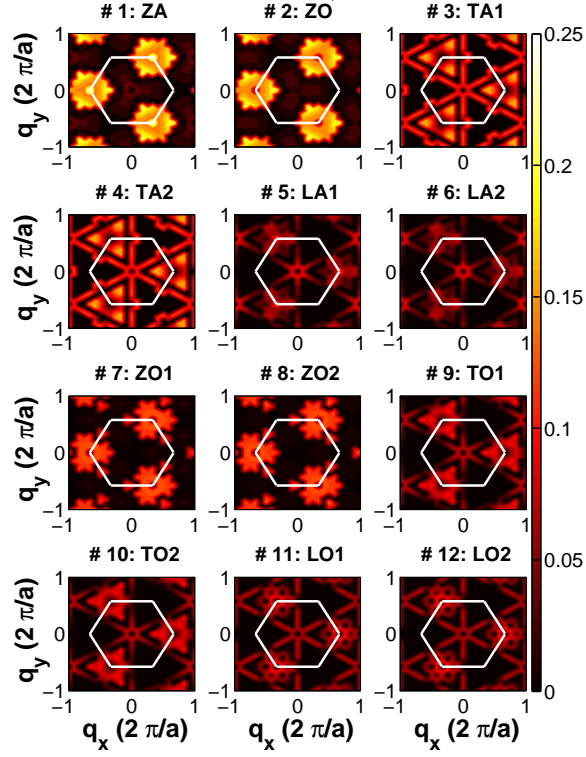


FIG. 2: (Color online) Intraband (π_1^*) matrix elements $\left| g_{\mathbf{k}+\mathbf{q},\mathbf{k}}^{(\pi_1^*,\pi_1^*)\nu} \right|$ (in units of eV) calculated by DFPT for \mathbf{k} at the conduction band minimum (i.e., the Dirac point) as a function of phonon wavevector \mathbf{q} and branch number ν . If compared to the matrix elements of MLG, the main difference is the absence of Kohn anomalies - sharp peaks in $\mathbf{q} = \mathbf{K}$ (TO1, TO2) and $\mathbf{q} = 0$ (LO1, LO2).

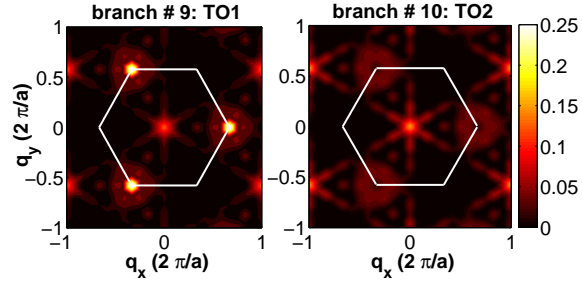


FIG. 3: Interband matrix elements ($\pi_1^* \rightarrow \pi_2^*$) (in units of eV) for phonon branches TO1 and TO2 ($\mathbf{k} = K$). The Kohn anomalies are clearly visible in a form of sharp peaks. The observed picture agrees with the selection rules for electron-phonon interaction in BLG. [13]

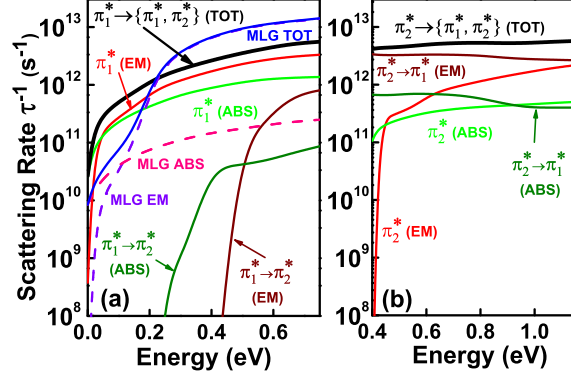


FIG. 4: (Color online) Scattering rates at $T = 300$ K as a function of electron energy $E_{\mathbf{k}}$, in BLG. The results are rather different depending on whether the electron is initially in the conduction band π_1^* (a), or π_2^* (b). In the former case, the dominance of the intraband (π_1^*) scattering is clear. The scenario when the electron is initially in π_2^* becomes more relevant when the gate bias is applied.